OPTICAL COMMUNICATION NETWORKS, DEVICES AND SENSORS

OPTICAL COMMUNICATION NETWORKS, DEVICES AND SENSORS

EDITED BY
MOHD RASHIDI SALIM
ARNIDZA RAMLI

Penerbit UTM Press
UNIVERSITI TEKNOLOGI MALAYSIA
www.penerbit.utm.my
2022

First Edition 2022

Perpustakaan Negara Malaysia Cataloguing-in Publication Data

OPTICAL COMMUNICATION NETWORKS, DEVICES AND SENSORS / Edited by Mohd Rashidi Salim, Arnidza Ramli.
ISBN 978-983-52-1863-7
1. Optical communications.
2. Optical fiber communication.
3. Optical detectors.
4. Government publications--Malaysia.
I. Mohd Rashidi Salim. II. Arnidza Ramli
621.3827

Editor: **MOHD RASHIDI SALIM & ARNIDZA RAMLI**
Editor Penyelaras/ Acquisition Editor: **NUR'AINA OSMAN**
Pereka Kulit / *Cover Designer:* **HAFIZAH MOHAMAD AHYAH**

Diatur huruf oleh / *Typeset by*
MOHD RASHIDI SALIM & ARNIDZA RAMLI
School of Electrical Engineering, Faculty of Engineering
UTM Johor Bahru

Diterbitkan di Malaysia oleh / *Published in Malaysia by*
PENERBIT UTM PRESS
Universiti Teknologi Malaysia
81310 UTM Johor Bahru
Johor Darul Ta'zim, MALAYSIA
(PENERBIT UTM ahli MAJLIS PENERBITAN ILMIAH MALAYSIA (MAPIM) dan anggota PERSATUAN PENERBIT BUKU MALAYSIA (MABOPA)
dengan no. keahlian 9101)

Dicetak di Malaysia oleh / *Printed in Malaysia by*
JASAMAX ENTERPRISE
No. 16, Jalan Kebudayaan 2, Taman Universiti
81300 Skudai, Johor, MALAYSIA

Contents

List of Contributors

Abdul Hadi Sulaiman *Institut Kejuruteraan Kuasa, Universiti Tenaga Nasional, Selangor*

Abu Sahmah Mohd Supa'at *Sekolah Kejuruteraan Elektrik, Fakulti Kejuruteraan, Universiti Teknologi Malaysia, Johor Bahru*

Ahmad Sharmi Abdullah *Sekolah Kejuruteraan Elektrik, Fakulti Kejuruteraan, Universiti Teknologi Malaysia, Johor Bahru*

Arnidza Ramli *Sekolah Kejuruteraan Elektrik, Fakulti Kejuruteraan, Universiti Teknologi Malaysia, Johor Bahru*

Asrul Izam Azmi *Sekolah Kejuruteraan Elektrik, Fakulti Kejuruteraan, Universiti Teknologi Malaysia, Johor Bahru*

Azura Hamzah *Malaysia-Japan International Institute of Technology (MJIIT), Universiti Teknologi Malaysia, Kuala Lumpur*

Fadila Mohd Atan *Fakulti Kejuruteraan Elektrik, Universiti Teknologi MARA, Kampus Pasir Gudang, Johor*

Hadi Manap *Fakulti Teknologi Kejuruteraan Elektrik dan Elektronik, Universiti Malaysia Pahang*

Hummad Habib Qazi *Sekolah Kejuruteraan Elektrik, Fakulti Kejuruteraan, Universiti Teknologi Malaysia, Johor Bahru*

Ian Yulianti *Faculty of Mathematics and Natural Sciences, Universitas Negeri Semarang, Indonesia*

Khairul Zafri Mustafa *Sekolah Kejuruteraan Elektrik, Fakulti Kejuruteraan, Universiti Teknologi Malaysia, Johor Bahru*

Nadiatulhuda Zulkifli *Sekolah Kejuruteraan Elektrik, Fakulti Kejuruteraan, Universiti Teknologi Malaysia, Johor Bahru*

Nelidya Md Yusoff *Fakulti Teknologi & Informatik Razak, Universiti Teknologi Malaysia, Kuala Lumpur*

Ngurah Made Darma Putra *Faculty of Mathematics and Natural Sciences, Universitas Negeri Semarang, Indonesia*

Nik Noordini Nik Abd Malik *Sekolah Kejuruteraan Elektrik, Fakulti Kejuruteraan, Universiti Teknologi Malaysia, Johor Bahru*

Ninik Irawati *Malaysia-Japan International Institute of Technology (MJIIT), Universiti Teknologi Malaysia, Kuala Lumpur*

CHAPTER 8

Plastic Optical Fiber Mach-Zehnder Interferometer for Intensity-based Refractive Index Sensor

Ian Yulianti, Ngurah Made D. P., Zunita Aryani Fahma Latif, and Abu Sahmah Mohd Supa'at

8.1 INTRODUCTION

Optical fiber sensors have attracted attention due to their advantages, such as resistance to electromagnetic interference, light in weight, small in size, small transmission attenuation, fast response, flexible geometry, and large bandwidth. Fiber optic sensors can be applied in high voltage, high temperature, or corrosive environments. Moreover, the optical fiber sensor can be implemented for remote monitoring. Fiber optic sensors has been proposed for various measurements, such as strain (Chen *et al*., 2021), displacement (Ghaffar *et al*., 2021), refractive index (Zheng *et al*., 2021), temperature (Su *et al*., 2021), pressure (X. Li *et al*., 2020) and biosensor (Xu, Xiong, and Yan 2021).

Refractive index is one of the important parameters in many applications such as biomedical, biochemical, food and

Optical Communication Networks, Devices, and Sensors
Edited by Mohd Rashidi Salim and Arnidza Ramli

environmental industries. Various methods have been developed to design fiber optic refractive index sensor, such as surface plasmon resonance (SPR) method (W. Li *et al*., 2020; Zhang *et al*., 2018), Fabry-Perot interferometer (Huang *et al*., 2020), evanescent wave (Samavati *et al*., 2019) and Mach-Zehnder interferometer (MZI) (Wu *et al*., 2021). Among those methods, MZI has advantages of good linearity, low cost, compact size and simple fabrication process.

The principle of MZI refractive index sensor is by observing the wavelength shift of the output spectrum due to the change of the environmental refractive index. MZI refractive index sensors have been reported using single mode silica optical fiber (SMF) by implementing various structures. Bhardwaj and Singh (2016) fabricated MZI in SMF by cascading two tapers using a fusion splicer. It was obtained that the sensitivity was 380nm/RIU. Melo *et al.* (2016) obtained a refractive index sensor with a sensitivity of 1307 nm/RIU by using a Mach-Zehnder interferometer coated with hafnium oxide. Other SMF-based MZI was proposed by Wang *et al.* (2016). The MZI was constructed from photonic crystal fiber (PCF) spliced in between two segments of SMF resulting in sensitivity of 260.8 nm/RIU. It is clear that the SMF-MZI has advantage of high sensitivity. Moreover, it also offers high reproducibility and large operational range. However, the SMF MZI has low mechanical strength. Jasim *et al*. (2014) has proposed MZI using graded-index (GI) plastic optical fiber (POF) by forming two tapers using heat-and-pull technique. The advantages of POF are that it has higher dimension and high mechanical strength than the SMF. Nevertheless, it has drawback of low sensitivity. It was found that the proposed GI-POF based MZI has a sensitivity of only 3.44 nm/RIU.

Beside exploiting the wavelength shift, measurement using MZI can also be conducted by observing the change of the output intensity. The advantage of adopting MZI for intensity modulation-based sensor is that it can improve the sensitivity. Moreover, by using MZI, the intensity measurement can be performed at two different wavelengths. Dual-wavelength measurement method

could be applied to overcome the drawback of the intensity-based sensor which is strongly influenced by intensity fluctuations which further limits its accuracy (Tapetado *et al*., 2014). Therefore, in this work, we proposed an intensity-based POF-MZI sensor for refractive index by implementing a dual-wavelength measurement method. Characterization and analyses were conducted in terms of sensitivity, linearity, hysteresis and accuracy.

8.2 PLASTIC OPTICAL FIBER MACH-ZEHNDER INTERFEROMETER

MZI sensor is a phase modulation sensor using a two-beam interferometer. The input light is separated into two parts which are the reference path and the sensing path, as shown in Figure 8.1. The reference path is the path covered with an insulated shield, while the sensing path is the sensing area exposed to external factors such as temperature, refractive index, and strain. After being separated for a certain distance, the reference path and the sensing part are then recombined. Once the light is recombined, interference occurs due to the phase difference.

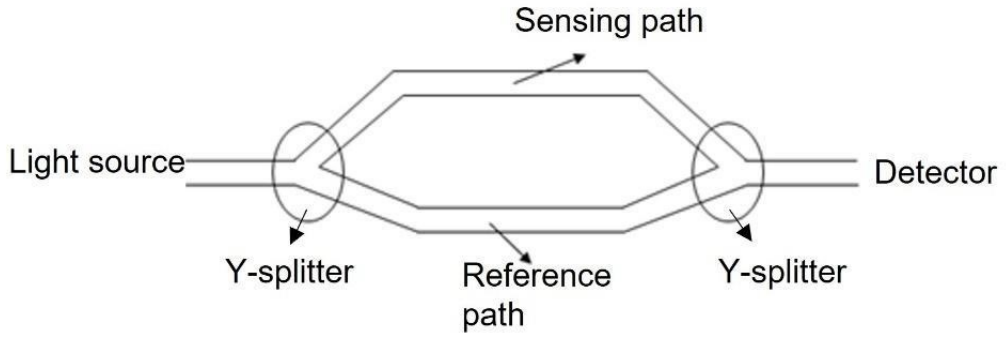

Figure 8.1 Structure of basic Mach-Zehnder Interferometer

Intrinsic MZI could be realized using POF by forming two tapers separated at certain distance. POF has advantage of having large core diameter which is around 1 mm. This large diameter

makes POF more durable and flexible than fiber glass. One of the main disadvantages of POF is it has a much higher power loss compared to silica optical fiber. Due to its high-power loss, POF is not suitable for long distance communication system. Instead, POF is widely used in optical sensor applications.

MZI structure using POF is shown in Figure 8.2. The two tapers are separated by a distance L. The POF portion is heated and stretched to form taper. Coherent light source as sensor input propagates in the core mode. When the light pass through the first taper, the light split into the cladding while the rest continues to propagate in the core. The light that propagates inside the cladding has difference phase with that propagates inside the core due to the difference of the refractive index. The light is then recombined at the second taper. The recombined light intensity is defined by (Jasim *et al*., 2014)

$$I_{out} = I_1 + I_2 + 2\sqrt{I_1 I_2}\, cos\, cos\, \Delta\emptyset \tag{8.1}$$

where I_1, I_2, $\Delta\phi$ are the intensity of light propagates at core, the intensity of light propagates at cladding and the phase difference between core mode and cladding modes, respectively. The phase difference depends on the effective refractive index of the core (n_{core}), and effective refractive index of the cladding (n_{clad}) and also the wavelength of the light (λ) as defined by

$$\Delta\emptyset = \frac{2\pi}{\lambda}\Delta N_{eff} L \tag{8.2}$$

where ΔN_{eff}=n_{clad}-n_{core} and L is the interferometer length. From equation (8.2), it is shown that the intensity of the transmitted light at certain wavelength highly depends on the effective refractive index of the core and the cladding. Since the cladding exposed to the environment, then its effective refractive index value change as the environment refractive index changes. Therefore, by observing the change of intensity at certain wavelength, the environment refractive index can be determined. To eliminate the fluctuation of

the intensity due to other factors that commonly occurs in intensity-based sensor, we proposed dual-wavelength method.

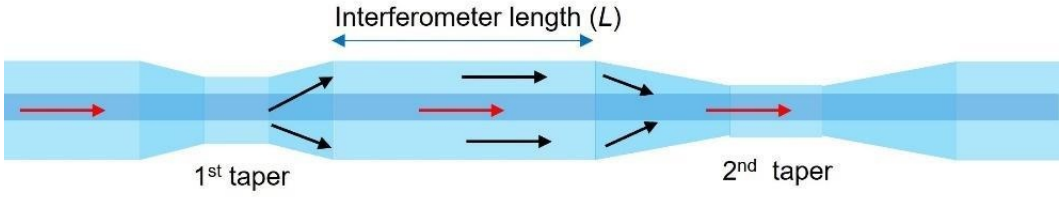

Figure 8.2 Intrinsic MZI structure

8.3 METHOD

The intrinsic MZI was fabricated using step index (SI) POF with core diameter of 980 µm (CC2-1000, Sichuan Huiyuan Plastic Optical Fiber Co., Ltd.). The core material and cladding material refractive index are 1.49 and 1.41, respectively. The core material of the POF is PMMA, while the cladding material is fluorinated polymer. The first step of the MZI fabrication was removing the polyethylene jacket of the POF using fiber stripper. To remove any excess dirt, the POF was then cleaned using alcohol. The two ends of the POF were attached to SMA 905 connector (Industrial Fiber Optics, Inc) after polished them using fiber optic sandpaper. Tapers were obtained by heating the POF using solder at temperature of 80^{o}C (Jasim *et al*., 2014). The distance of the two tapers is 1 cm. Measurement of the taper waist diameters were done by using CCD-optical microscope.

The sensor response to the environment refractive index change was characterized by immersing the MZI-POF in glucose solution. The glucose concentration was varied with an increment of 2% in the range of 0% to 12% at room temperature which correspond to the refractive index of 1.3330 to 1.3547 (measured using ABBE refractometer). Light was launched at the one end of the POF, so that it propagates through the MZI. As a light source, a

light emitting diode (LED) having wavelength of 430 nm and bandwidth of 80 nm was used. At the other end, the POF was connected to a spectrometer (Ocean Optics UV-VIS), so that the output spectrum could be recorded. The characterization set-up is shown in Figure 8.3.

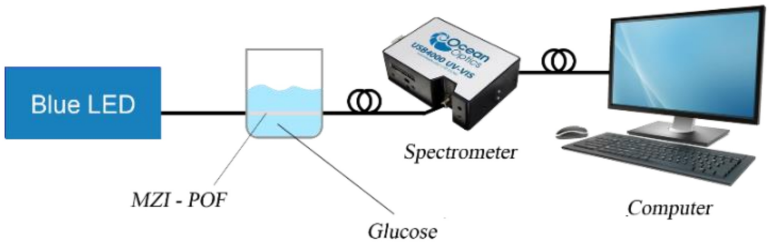

Figure 8.3 Equipment set up for characterization of the sensor

8.4 RESULTS AND DISCUSSIONS

The fabricated MZI is shown in Figure 8.4 (a) and the images obtain from CCD microscope are shown in Figure 8.4 (b) and Figure 8.4 (c). It is shown that two tapers have been formed on the POF. The first taper and the second taper diameters are 533.783 and 690.74 µm respectively. It is shown that the first taper is sharper than the second taper to allow excitation of cladding modes. Meanwhile, the smooth second taper was designed to reduce loss when the light recombine.

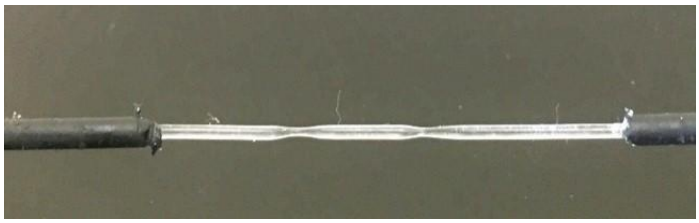

(a)

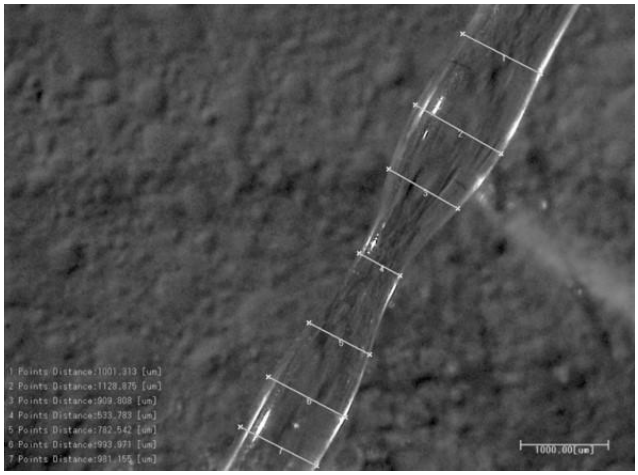

(b)

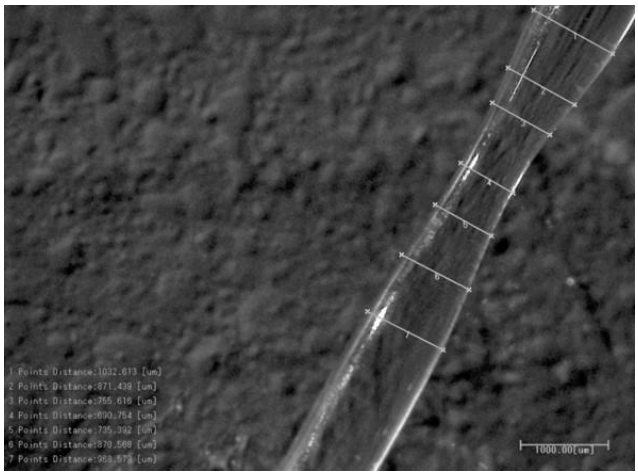

(c)

Figure 8.4 (a) The fabricated MZI, (b) microscope image of the first taper and (c) microscope image of the second taper

The transmittance of the MZI in the air and in distilled water are shown in Figure 8.5. It is observed that the spectra show interference pattern with three dips and two peaks. The dips occurred at wavelength of 424 nm (λ_1), 462.64 nm (λ_3), and 519.48 nm ($(\lambda_5$), whereas the peaks occurred at 437.14 nm (λ_2) and 478.77 nm (λ_4). It is also shown that the transmittances in distilled water are lower than that in the air. The lower transmittance occurred due to the influence of the refractive index of the distilled water which

is higher than the refractive index of the air. This result agrees with the Snell's law that states that higher cladding refractive index results in higher critical angle. Hence, more light will be refracted to the cladding region which further causes the decrease of the transmittance. The same results also obtained when the MZI was characterized in various refractive index solutions, as shown in Figure 8.6. As the refractive index increased, the transmittance decreased for all wavelength range.

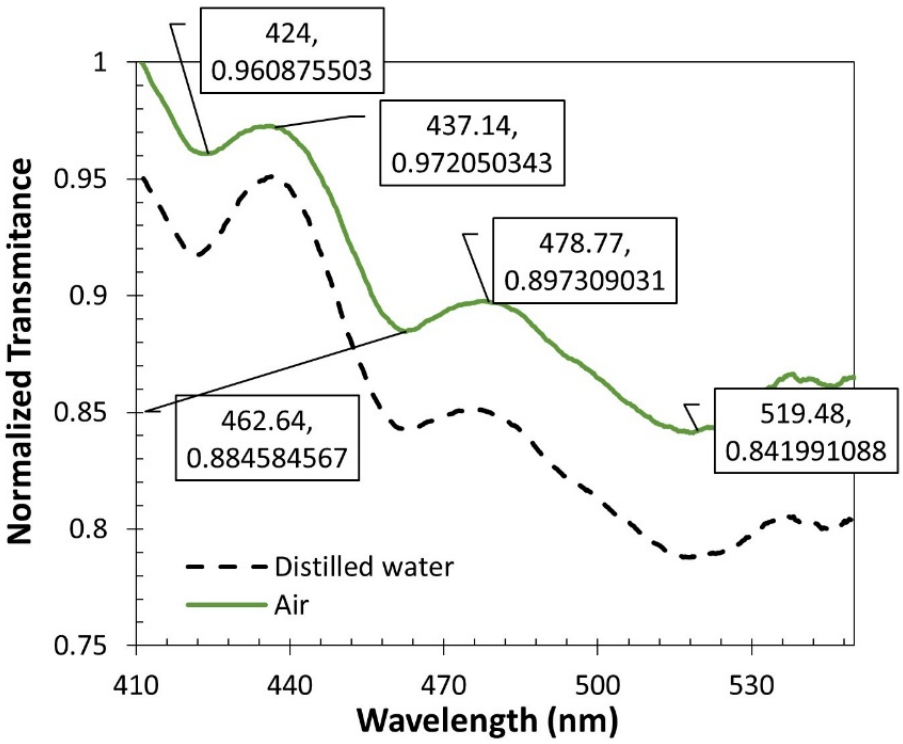

Figure 8.5 Spectra of the MZI in the air and in distilled water

8.4.1 Sensitivity and Linearity

Dual-wavelength method was realized by taking the transmittance ratio of two wavelengths. For this purpose, the above-mentioned wavelength of the dips and the wavelength of peaks were used. Ten wavelength pairs were compared and analyzed to obtain the best performance in terms of sensitivity and linearity. The wavelength

pairs were λ_1/λ_2, λ_1/λ_3, λ_2/λ_3, λ_1/λ_4, λ_2/λ_4, λ_3/λ_4, λ_1/λ_5, λ_2/λ_5, λ_3/λ_5 and λ_4/λ_5. The transmittance ratios were calculated from the spectra of the MZI output in various refractive index solutions which is shown in Figure 8.6.

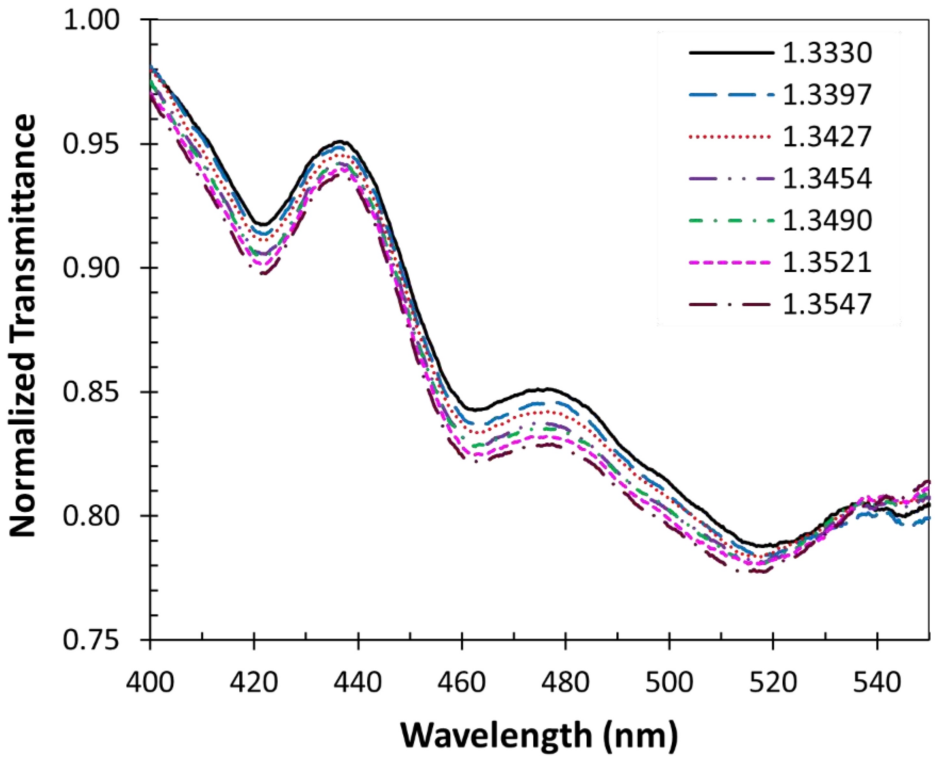

Figure 8.6 Spectra of the MZI output in various refractive index solutions

To obtain the refractive index sensitivity and the linearity response of the MZI, the calculated transmittance ratios were plotted against the refractive index values. The results showed that from all wavelength pairs, there are six pairs that have good linearity, as indicated by correlation factor of above 0.9, which arranged from the highest are λ_2/λ_4, λ_1/λ_2, λ_2/λ_3, λ_1/λ_4, λ_3/λ_5, and λ_4/λ_5 as shown in Table 8.1. The highest linearity was 0.9979 which is occurred at wavelength of λ_2/λ_4 with sensitivity of 0.6336/refractive index unit

(RIU). Meanwhile, in terms of sensitivity, the highest six wavelength pairs are λ_4/λ_5, λ_3/λ_5, λ_2/λ_4, λ_2/λ_3, λ_1/λ_4 and λ_1/λ_2.

Table 8.1 Sensitivity and linearity of the MZI of various wavelength pairs

Wavelength pairs	Absolute Sensitivity values (/RIU)	Correlation factor (R^2)
λ_1/λ_2	**0.2877**	**0.9579**
λ_1/λ_3	0.1790	0.5873
λ_2/λ_3	**0.5151**	**0.9576**
λ_1/λ_4	**0.2880**	**0.9511**
λ_2/λ_4	**0.6336**	**0.9979**
λ_3/λ_4	0.1083	0.4886
λ_1/λ_5	0.5298	0.8656
λ_2/λ_5	0.1897	0.4090
λ_3/λ_5	**0.6506**	**0.9256**
λ_4/λ_5	**0.7732**	**0.9249**

By considering both sensitivity and linearity, wavelength pairs of λ_2/λ_3 and λ_2/λ_4 were selected for further analysis since they provide moderate sensitivity and high linearity. Linearity is important since it determines the sensor accuracy. The transmittance ratio graphs for λ_2/λ_3 and λ_2/λ_4 are shown in Figure 8.7. It is shown that the transmittance ratio increased as the refractive index increased. However, as expected, the transmittance at single wavelength, decreased as the refractive index increased. The transmittances at wavelength of λ_2, λ_3, and λ_4 for various refractive index are shown in Figure 8.8. From Figure 8.8, it is also noticed that the single-wavelength methods showed high linearity with correlation factor of above 0.96 as well as high sensitivity. The highest sensitivity and linearity showed at the measurement at λ_4, which are -1.0481/RIU and 0.9851, respectively. Good sensitivity and linearity at single-wavelength method contribute to the high sensitivity and linearity of the dual-wavelength method.

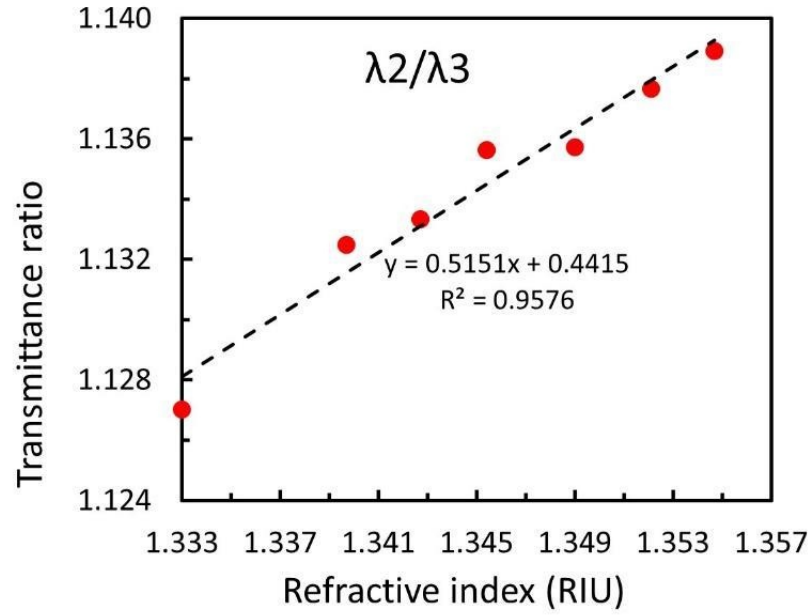

(a)

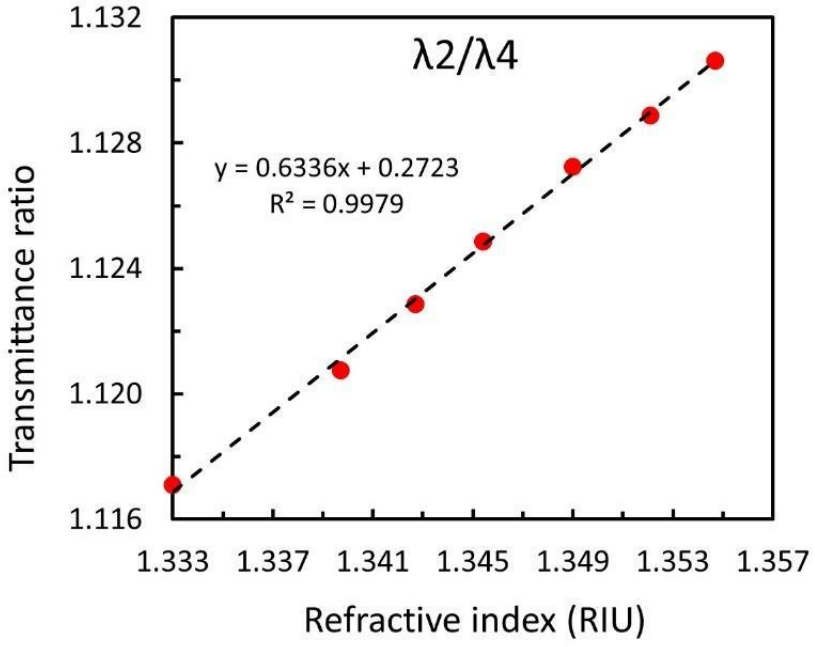

(b)

Figure 8.7 Transmittance ratio of the MZI vs. refractive index for (a) λ_2/λ_3 and (b) λ_2/λ_4

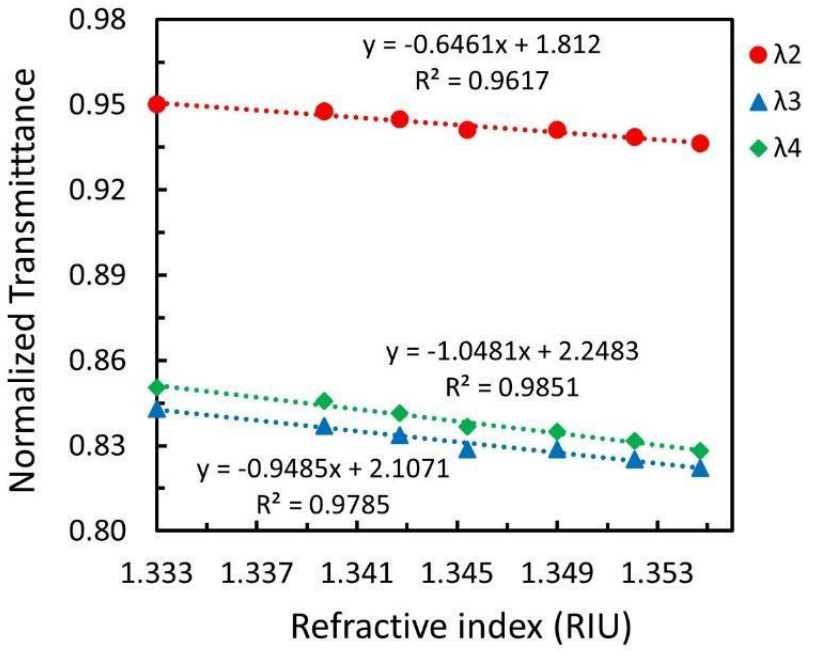

Figure 8.8 Normalized transmittance of the MZI vs. refractive index for λ_2, λ_3 and λ_4

8.4.2 Hysteresis and Accuracy

Hysteresis characterization was done by performing reverse measurement from the highest refractive index to the lowest. The results of a full cycle measurement at λ_2/λ_3 and λ_2/λ_4 are shown in Figure 8.9. Total hysteresis error (H) is the maximum hysteresis error across the full cycle as defined by (Avila-Garcia et al. 2018)

$$H = \Big(\big(I(i) - D(i) \big) / I(i) \Big) \tag{8.3}$$

where $I(i)$ and $D(i)$ are the transmittance ratio from the increasing measurement and the decreasing measurement of the i^{th} data, respectively. Calculation results showed that λ_2/λ_3 has lower hysteresis error than λ_2/λ_4. The values of the hysteresis error for λ_2/λ_3 and λ_2/λ_4 are 8.67×10^{-4} and 1.857×10^{-3} respectively. Beside nonlinearity, hysteresis is another factor that contributes to the sensor accuracy.

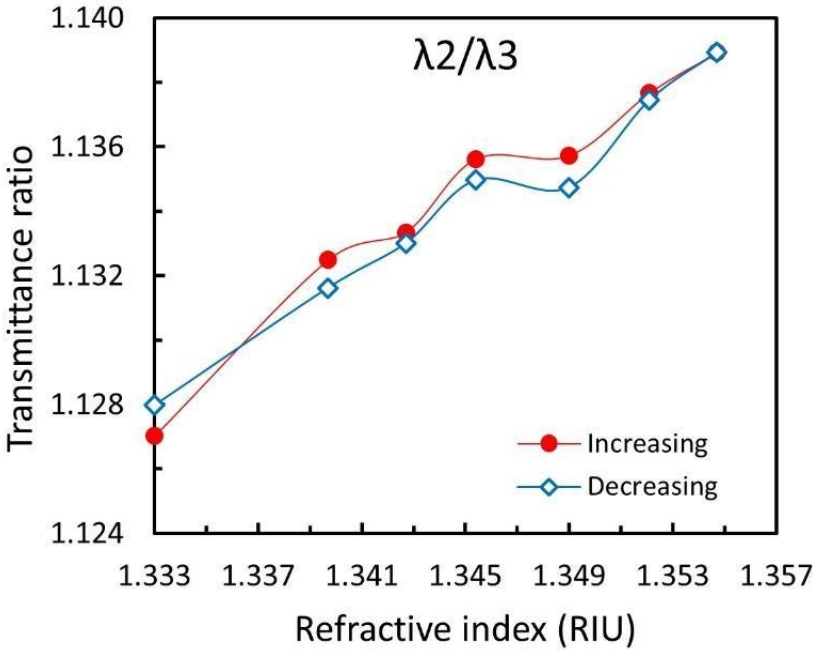

(a)

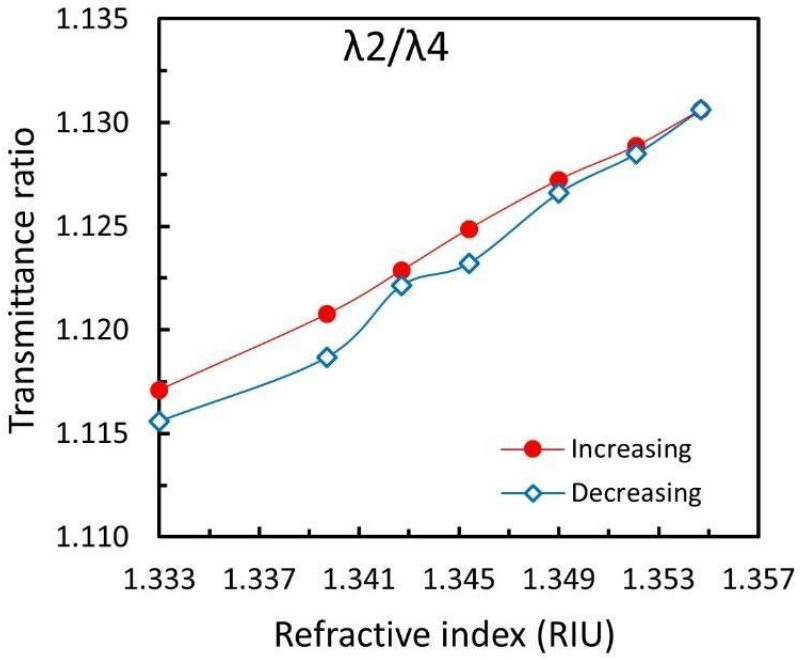

(b)

Figure 8.9 Hysteresis curve of dual-wavelength method at (a) λ_2/λ_3 and (b) λ_2/λ_4

For comparison, hysteresis of single-wavelength method was also analyzed. Hysteresis of measurement at λ_4 was used since it has the highest sensitivity and linearity. The hysteresis curve of measurement at λ_4 is shown in Figure 8.10. The total hysteresis obtain from calculation is 4.212×10^{-3}. Therefore, the dual-wavelength measurement provides better hysteresis compared to the single-wavelength method. Hysteresis improvement obtained by using wavelength pair of λ_2/λ_3 and λ_2/λ_4 are 79.4% and 55.9%, respectively.

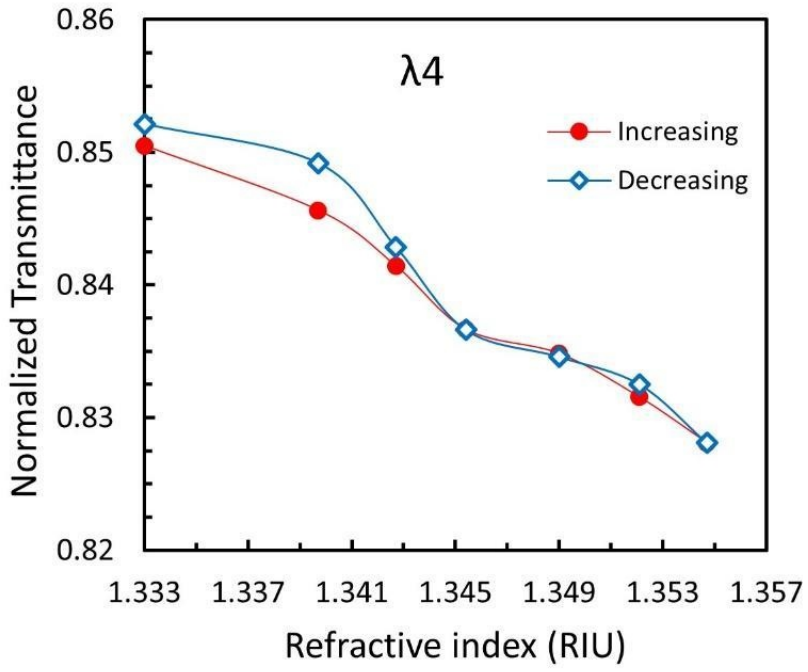

Figure 8.10 Hysteresis curve of single-wavelength method at λ_4

To investigate the accuracy, the refractive index obtained from dual-wavelength methods were calculated using the linear regression equation obtained from graphs in Figure 8.9(a) and (b), as defined by

$$n_1 = \frac{Tr-0.4415}{0.5151} \tag{8.4}$$

$$n_2 = \frac{Tr - 0.2723}{0.6336} \tag{8.5}$$

where n_1 and n_2 are the refractive index obtained using wavelength pair of λ_2/λ_3 and using wavelength pair of λ_2/λ_4, respectively. Whereas Tr is the transmittance ratio obtained from the measurement. The accuracy is obtained by calculating the relative error of the measured refractive index compared to the actual refractive index (the actual refractive index of the glucose solution measured by using ABBE refractometer). The accuracy of the single-wavelength method was also calculated for comparison purpose. The measured refractive index using wavelength of λ_4 (n_3) is defined by the regression linear equation obtained in Figure 8.8, which is

$$n_3 = \frac{Tr - 2.2483}{1.0481}. \tag{8.6}$$

The relative errors of twice measurement using dual-wavelength and single wavelength method are shown in Figure 8.11. It is shown that, by using single wavelength method, the relative errors of the two cycles are different in significant values. It is indicated that the single wavelength method is highly affected by the transmittance fluctuation during measurement. The highest relative errors of all measurement of the single wavelength method are 0.357%. Meanwhile, for the dual-wavelength method, the highest relative errors are 0.235% and 0.291% for λ_2/λ_3 and λ_2/λ_4, respectively. Therefore, the accuracy improvement of the dual wavelength method is 34.21% and 18.64% for λ_2/λ_3 and λ_2/λ_4, respectively. Clearly, the higher sensor accuracy was achieved by implementing wavelength pair of λ_2/λ_3. This result is in line with the result of the hysteresis analysis, and it is acceptable since the more hysteresis error is reduced, the higher the accuracy is.

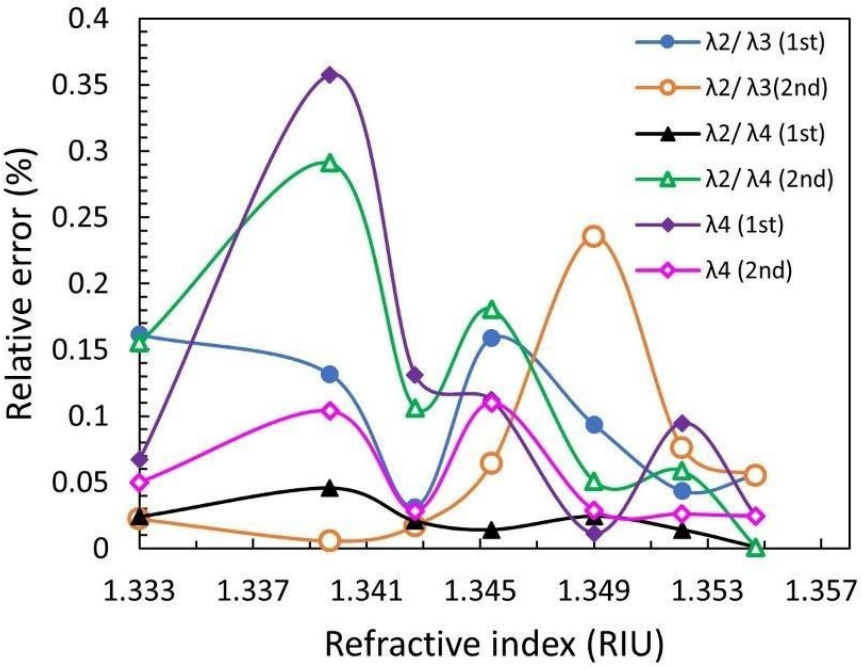

Figure 8.11 Relative error of dual-wavelength and single-wavelength method for two cycle measurement

8.5 CONCLUSION

Intensity-based MZI sensor for refractive index measurement using SI-POF has been fabricated by forming two tapers. The measurement method was done by using dual wavelength to improve the sensor accuracy. The results showed that by using the proposed dual-wavelength method, the hysteresis error was significantly reduced to 79.4%. As consequence, the sensor accuracy was improved with improvement up to 34.21%. The highest improvement was achieved at wavelength pair of λ_2/λ_3.

ACKNOWLEDGEMENT

We would like to thank to Ministry of Education and Culture, Indonesia for funding the research through grant no 19.25.3/UN37/PPK.6.8/2021. Our gratitude also goes to the

members of Physics Department, Universitas Negeri Semarang for their helpful discussion throughout the completion of this work.

REFERENCES

Avila-Garcia, M.S. *et al*. 2018. "High Sensitivity Strain Sensors Based on Single-Mode-Fiber Core-Offset Mach-Zehnder Interferometers." *Optics and Lasers in Engineering,* 107: 202–206.

Bhardwaj, V, and V. K. Singh. 2016. "Fabrication and Characterization of Cascaded Tapered Mach-Zehnder Interferometer for Refractive Index Sensing." *Sensors and Actuators: A. Physical,* 244: 30–34.

Chen, H. *et al*. 2021. "Bubble Microcavity Strain and Gravity Sensor with Temperature and Bending Insensitivity Using an Ultra-Thin Core Optical Fiber." *Optics and Laser Technology,* 142: 107193.

Ghaffar, A. *et al*. 2021. "A Novel Sensor Design for Displacement Measurement Using Plastic Optical Fiber-Based on Face-Coupling Method." *Optical Fiber Technology,* 67: 102684.

Huang, L. *et al*. 2020. "Optical Fiber Fabry-Perot Interferometer Refractive Index Sensor Based on Vernier Effect for Silica Colloidal Sol Aging Monitoring." *Optical Fiber Technology,* 60: 102338.

Jasim, A. A. *et al*. 2014. "Refractive Index and Strain Sensing Using Inline Mach-Zehnder Interferometer Comprising Perfluorinated Graded-Index Plastic Optical Fiber." *Sensors and Actuators, A: Physical,* 219: 94–99.

Li, W. *et al*. 2020. "Theoretical Analysis on SPR Based Optical Fiber Refractive Index Sensor with Resonance Wavelength Covering Communication C+L Band." *Optik,* 213: 164696.

Li, X. *et al*. 2020. "A New Type of Structure of Optical Fiber Pressure Sensor Based on Polarization Modulation." *Optics and Lasers in Engineering,* 130: 106095.

Melo, L., G. Burton, P. Kubik, and P. Wild. 2016. "Refractive Index Sensor Based on Inline Mach-Zehnder Interferometer Coated with Hafnium Oxide by Atomic Layer Deposition." *Sensors and Actuators, B: Chemical,* 236: 537–545.

Samavati, Z. *et al*. 2019. "Comprehensive Investigation of Evanescent Wave Optical Fiber Refractive Index Sensor Coated with ZnO Nanoparticles." *Optical Fiber Technology,* 52: 101976.

Su, H. *et al*. 2021. "High-Sensitivity Optical Fiber Temperature Sensor with Cascaded Configuration of MZI and FPI Based on Vernier Effect." *Optical Fiber Technology,* 67: 102751.

Tapetado, A. *et al*. 2014. "Self-Referenced Temperature Sensor Based on a Polymer Optical Fiber." 23rd International Conference on Optical Fibre Sensors. Santander, 2-6 June.

Wang, Q. *et al*. 2016. "High Sensitivity Refractive Index Sensor Based on Splicing Points Tapered SMF-PCF-SMF Structure Mach-Zehnder Mode Interferometer." *Sensors and Actuators, B: Chemical,* 225: 213–220.

Wu, Y. *et al*. 2021. "Improved Optical Fiber Mach-Zehnder High-Sensitivity Refractive Index Sensor." *Optik,* 229: 166214.

Xu, Y., M. Xiong, and H. Yan. 2021. "A Portable Optical Fiber Biosensor for the Detection of Zearalenone Based on the Localized Surface Plasmon Resonance." *Sensors and Actuators B: Chemical,* 336: 129752.

Zhang, Z. *et al*. 2018. "Groove Micro-Structure Optical Fiber Refractive Index Sensor with Nanoscale Gold Film Based on Surface Plasmon Resonance." *Optical Fiber Technology,* 43: 45–48.

Zheng, Y., X. Yang, W. Feng, and W. Fan. 2021. "Optical Fiber Refractive Index Sensor Based on SMF-TCF-NCF-SMF Interference Structure." *Optik,* 226: 165900.